

Automated concrete exposed reinforcement and corrosion detection and measurement using coloured illumination

Hamish Dow^{1*}, Andrew Darby¹, Marcus Perry¹, and Feng Zhang¹

¹Department of Civil and Environmental Engineering, University of Strathclyde, G1 1XJ, UK

Abstract. Visual identification of reinforced concrete structure defects is vital to ensuring structural longevity and resilience. This paper explores the use of selective reflection imaging for concrete surface corrosion and exposed reinforcement detection and measurement. Selective reflection occurs when certain image colours are reflected more strongly than others by a surface. This effect can enhance colour contrast, making certain objects in a captured image appear darker. By imaging concrete surfaces using a blue lighting source, the contrast of red-coloured corrosion and exposed reinforcement is enhanced, particularly in greyscale images used by many defect detection algorithms. An inspection algorithm is proposed to segment these features using blue light images and Otsu thresholding, enabling accurate measurement of corrosion surface area. On laboratory slab samples, the algorithm obtained Intersection over Union (IoU) scores of over 84 % when compared to human-defined ground truths. Additionally, the algorithm's corrosion surface area measurements produced a maximum relative error of negative 8 %. These findings demonstrate how colour-controlled illumination can enhance visual inspections, leading to more efficient monitoring and improved durability of reinforced concrete structures.

1 Introduction

1.1 Background

Reinforced concrete is a popular construction material. However, due to environmental and physical conditions, many concrete structures degrade. A common defect is the loss of concrete cover (i.e. the concrete shielding the reinforcement) from reinforcement corrosion-induced spalling. As cover is reduced and the underlying reinforcement becomes exposed, corrosion can be accelerated as it comes into direct contact with moisture and air, weakening the structure [1]. An indication of this deterioration is visible reinforcement and corrosion surface staining. Figure 1 shows exposed reinforcement with minor corrosion staining on a concrete bridge column. Figure 2 illustrates a severely degraded reinforced concrete bridge column cap, showing exposed reinforcement and corrosion staining.

Regular inspections are vital to ensure a structure's safety and longevity. While traditional human-led visual inspections can be accurate, they often lack repeatability and expose human inspectors to hazardous environments, such as working at height.

Remote and automated inspections can remove physical risks to human inspectors and accelerate inspections. Many solutions exist, such as Light and Detection Ranging (LiDAR) and Terrestrial Laser Scanning (TLS). However, imaged-based solutions remain popular with asset inspectors and managers due to their low cost, ease of interpretation and accuracy [2] [3].

Remote visual inspections typically involve capturing image data with a camera mounted on a remote access device, such as a robot or unmanned aerial vehicle (UAV). However, human review of captured inspection data is monotonous and often error-prone [4]. Automated analysis techniques offer a more efficient alternative to identifying defects in remote inspection images.



Figure 1. Minor exposed reinforcement and corrosion on concrete bridge column.

* Corresponding author: hamish.dow@strath.ac.uk



Figure 2. Severely exposed reinforcement and corrosion staining of a concrete bridge column cap.

1.2 Automated corrosion detection

Image analysis can be conducted through white-box (image processing) and black-box (neural network) methods [5]. Çelik et al. [6], presented a black-box method for concrete corrosion segmentation in images. Using the semantic segmentation network EfficientNetB0, they achieved a corrosion Intersection over Union (IoU) score, a metric described in Section 3.3 of this paper, of 64 %. Çelik et al. commented on how poor image scene illumination led to false positive predictions from the model. Xu et al. [7], proposed a similar approach using the semantic segmentation network U-net, but achieved a corrosion IoU of only 8%.

Guru Prathap Reddy et al. [8], demonstrated a white-box method for quantifying concrete deterioration using image colour information, such as changes in image hue, saturation and intensity. By analysing concrete surface colour changes over time, they established empirical relationships to identify the attacking chemical, estimate the duration of exposure, and predict the remaining strength of the concrete.

Image scene illumination conditions can influence concrete defect detection and measurement results. Cho et al. [9], demonstrated how scene illumination could alter the results of human inspector measurements of concrete crack widths. McAlorum et al. [10] and Dow et al. [11], demonstrated how scene illumination angle of incidence can enhance the detection of concrete spalling and cracking, respectively.

1.3 Selective reflection

Selective reflection occurs when certain wavelengths (i.e. colours) of light are reflected more strongly than others by surfaces, owing to material interactions with specific energies of light. This can be used to increase the colour contrast of an image. Figure 3 demonstrates selective reflection using blue light to enhance the contrast of a red pen in a greyscale image.

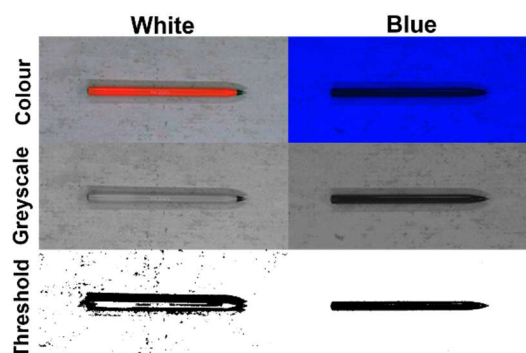


Figure 3. Demonstration of selective reflection with blue light on red pen.

Selective reflection is often used in industrial imaging applications [12]. Chen et al. [13], demonstrated how image scene illumination colour could be leveraged to enhance the quality of data captured for underwater concrete structures. As with the pen in Figure 3, concrete corrosion and exposed reinforcement are typically shades of red, and blue lighting will enhance their contrast. This contrast enhancement is advantageous for white-box image processing methods that utilise greyscale input images, such as Otsu thresholding. Monochrome cameras, which capture one-channel greyscale images, are commonly used in machine vision due to their high light sensitivity and detail (e.g. [14] [15]).

2 Proposed method

Figure 4 illustrates the proposed method. An image of the concrete surface is captured under blue lighting. Image processing techniques are then applied to segment the image into corroded and non-corroded pixels, allowing the corrosion area to be automatically calculated. The proposed algorithm is outlined in sections 2.1 – 2.4.

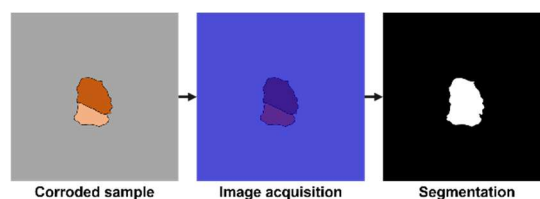


Figure 4. Flowchart of the proposed method using blue illumination to conduct segmentation of corrosion.

2.1 Image acquisition

Figure 5 provides a diagram of the hardware used to capture images for this work. In a controlled environment with no external light source, the concrete surface is illuminated using a blue ring light. Blue light was chosen because corrosion typically appears red due to iron oxide. By using blue illumination, no red light is present for the corrosion to reflect. Since corrosion absorbs blue light and reflects minimal amounts of it, it appears dark in the captured images. This enhances the

contrast between corroded and uncorroded areas, making segmentation more effective for automated analysis.

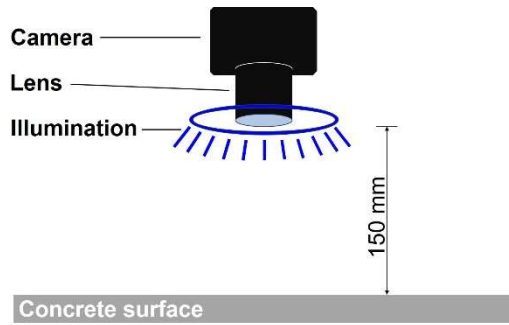


Figure 5. Image acquisition hardware used to capture images under blue illumination.

2.2 Image pre-processing

The captured colour image is converted to greyscale. Each pixel's RGB values are converted into a single intensity value that represents a weighted sum of the RGB values.

2.3 Automated corrosion segmentation

Otsu thresholding [16] is applied to segment the greyscale image into corroded (C) and un-corroded (UC) pixels based on greyscale pixel intensity. A threshold T is applied where if a pixel intensity is greater than T it is part of the UC class, if it is less than T it is part of the C class.

The Otsu thresholding method selects an optimum threshold T that maximises the intra-class variance in the image corroded and non-corroded pixels. The intra-class variance is defined in Equation 1.

$$\sigma^2(T) = \omega_C(T)\sigma_C^2(T) + \omega_{UC}(T)\sigma_{UC}^2(T)$$

Equation 1. Intra-class variance for Otsu thresholding.

Where: $\sigma_C^2(T)$ and $\sigma_{UC}^2(T)$ denote the variance of pixel intensities for each class; $\omega_C(T)$ and $\omega_{UC}(T)$ represent the probability of the number of pixels for each class at threshold T .

The threshold value is iteratively selected and the value that maximises the intra-class variance is selected. The final threshold value, T_{Final} , is then calculated using a value of 80 % of T , as shown in Equation 2.

$$T_{Final} = 0.8T$$

Equation 2. Threshold value taken as 80 % of Otsu's threshold.

The resulting binarised output image consists of white pixels (pixel intensity of 255) representing the corrosion class and black pixels (pixel intensity of 0) representing the non-corrosion class.

2.4 Surface area measurement

Surface area of corrosion is calculated to allow human inspector interpretability. As all images were captured from a fixed lens-to-surface distance of 150 mm, all images have dimensions of 211 mm × 177 mm, and a surface area of 37,388 mm². As the camera resolution is 2,448 × 2,048 pixels, the total number of pixels in the image is 5,013,504 pixels. This information is used to form Equation 3, which converts the total number of corroded pixels, $P_{corroded}$, in an image to surface area of corrosion in mm².

$$Corrosion\ area = \frac{37,388}{5,013,504} P_{corroded} (mm^2)$$

Equation 3. Corrosion segmentation pixels-to-mm² conversion.

3 Methodology

Analysis of the coloured lighting exposed reinforcement and corrosion detection method requires:

- formation of laboratory slabs;
- image acquisition;
- ground truth definition; and,
- outline of benchmarks and metrics.

3.1 Dataset formation

A laboratory dataset of concrete slab samples with dimensions of 300 mm × 300 mm × 30 mm (length × width × height) was created. The mix design of the concrete slabs is listed in Table 1 (in kg/m³). The cement used was grey CEM I 42.5 N cement, sourced from Hanson Ltd.

Table 1. Concrete slab mix design. All units are in kg/m³.

Cement	Sand	Coarse Aggregate	Water
400	800	1200	160

Several 6 mm diameter rebars were placed in the concrete to simulate reinforcement. Each rebar was connected to an insulated wire, which was exposed out of the concrete (see Figure 6a). The wire functioned as a conductor.

Additionally, to generate spalling on the newly cast samples, a 3D-printed model was inserted into each concrete mould (connected to the rebar) during the casting process (see Figure 6b). To ensure dataset variety, each slab's 3D print varied in size, shape and depth.

After curing and demoulding of the slabs, the 3D-printed inserts were removed. Accelerated corrosion was induced for each slab using the impressed current method for the slabs immersed in saltwater. In this process, a power supply of 30 V and 5 A was used, and the electrical current was applied to the rebars through the exposed wires (see Figure 6c).

After 30 minutes of accelerated corrosion, each slab was removed from the bath and dried. The resulting slab

shows corrosion staining in the spalled area, resembling a corroded spalling sample from a real-world structure (see Figure 6d). This process was repeated for all slabs in the dataset.

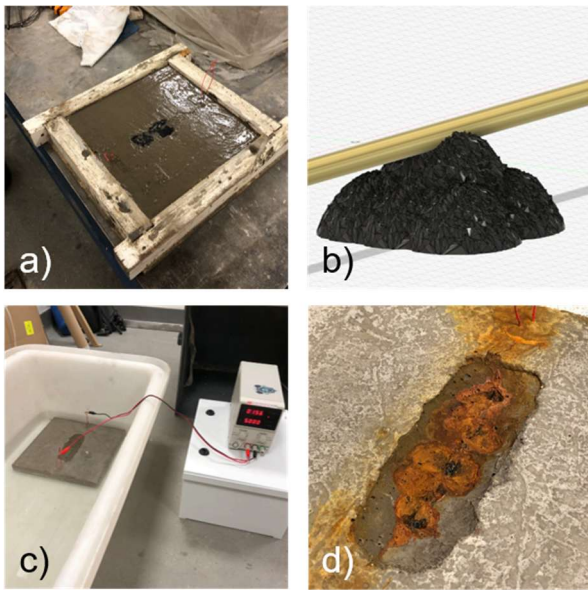


Figure 6. Corroded slab dataset formation process: a) casting of mould; b) 3D printed spalling inverse inserted into the concrete; c) accelerated corrosion using a salt bath; d) resulting corroded concrete.

3.2 Data acquisition and ground truth formation

For each slab sample, two images were captured from a fixed position. One with the concrete surface illuminated under white lighting and another under blue lighting. The image capture settings were manually controlled to ensure consistent illumination in both images.

A ground truth for each slab sample was then created by manually tracing the corroded area in software. Corroded areas were marked white with a pixel value of 255 (white) and un-corroded areas were marked with a pixel value of 0 (black).

3.3 Benchmarking methodology

Intersection over Union (IoU) was used to measure the performance of the corrosion segmentation method in comparison to the ground truths. IoU quantifies the overlap between the algorithm's output and the ground truth and is found using Equation 4.

$$IoU = \frac{TP}{TP + FP + FN}$$

Equation 4. Intersection over Union (IoU) metric calculation.

Where:

- TP (true positives): the number of corroded pixels in the ground truth correctly identified by the proposed algorithm.

- FP (false positives): the number of pixels the algorithm identified as corroded but were un-corroded in the ground truth.
- FN (false negatives): the number of pixels the algorithm identified as un-corroded but were labelled as corroded in the ground truth.

The surface area of corroded pixels in the ground truths was also calculated using an identical method to Section 2.4. IoU and surface area were calculated for each dataset sample.

4 Results and discussion

4.1 Image contrast enhancement

Figure 7a shows the corroded concrete when imaged under white lighting. The inset showcases a small sample of the surface and the corresponding greyscale image. Figure 7b shows the same image scene when illuminated using blue lighting. The insets for this figure show how the corroded concrete pixels are darker than the surrounding concrete; this is due to the blue light being absorbed (and not reflected) by the red-coloured corrosion staining in the image.

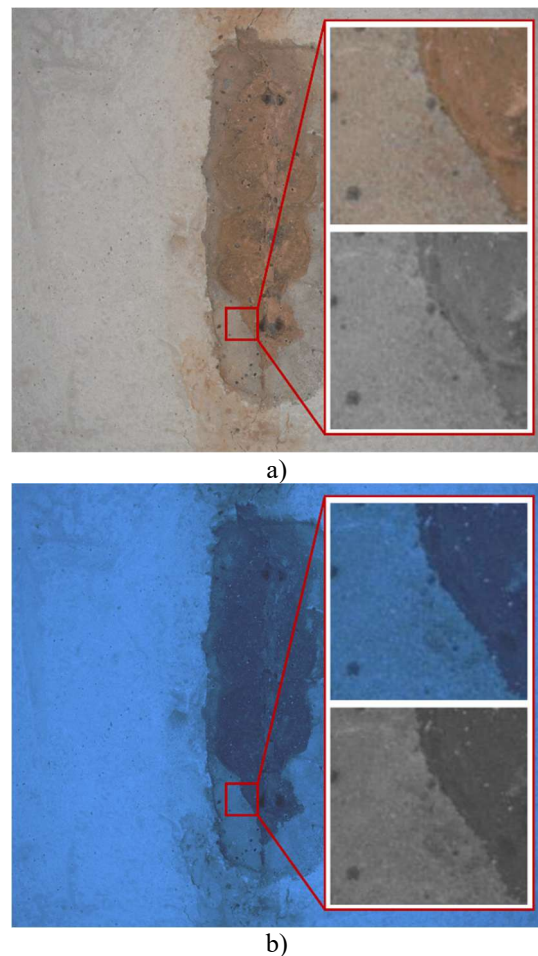


Figure 7. Sample 1 Concrete corrosion imaged under: a) white lighting; b) blue lighting. The greyscale image highlights how contrast is greater in the blue light image.

The enhanced contrast in the blue lighting image allows better delineation between the corrosion staining and the un-corroded concrete surface. These findings are consistent with sample 2, shown in Figure 8.

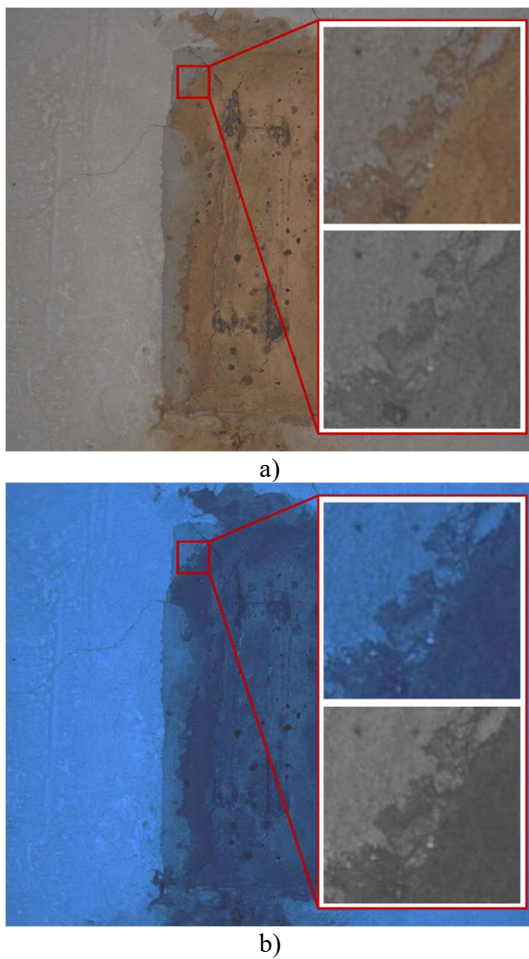


Figure 8. Sample 2 Concrete corrosion imaged under: a) white lighting; b) blue lighting. The greyscale image highlights how contrast is greater in the blue light image.

4.2 Qualitative and quantitative results

4.2.1 Dataset sample 1

Figure 9 illustrates the proposed method output, ground truth and corresponding intersection over union result.

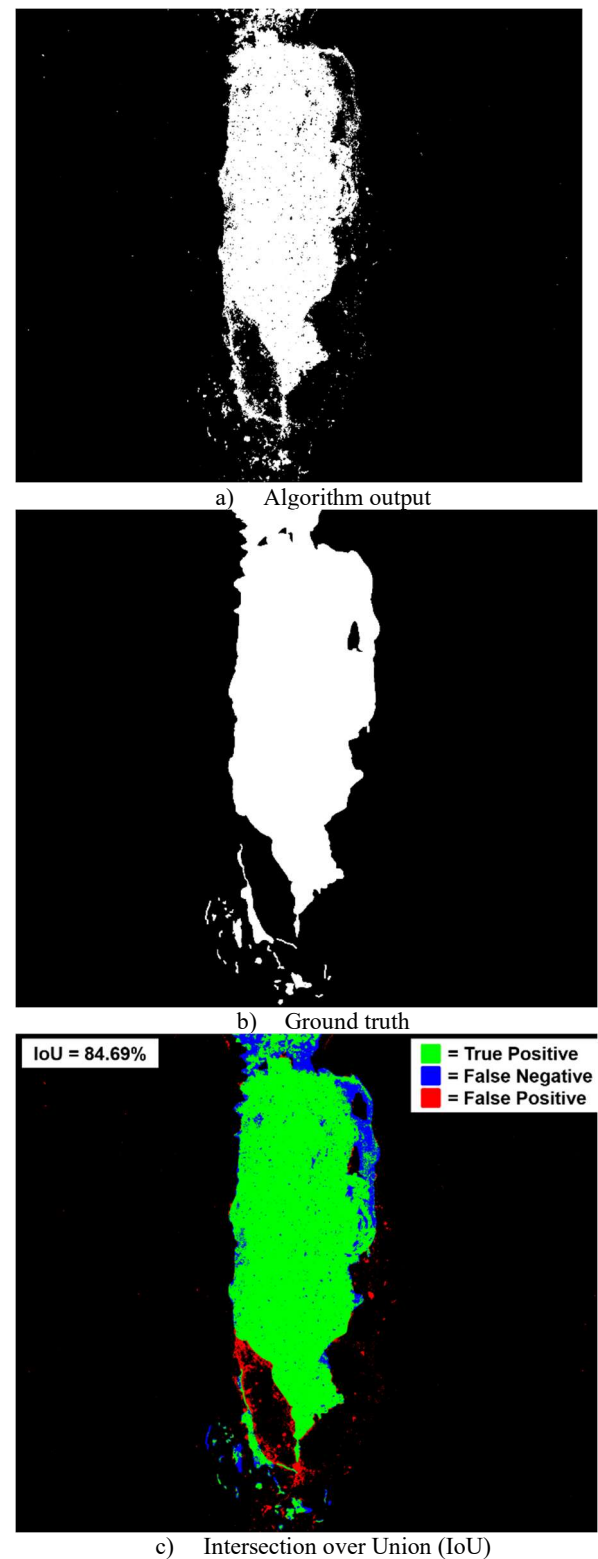


Figure 9. Results for dataset sample 1: a) Algorithm output b); Ground truth; c) Intersection over Union (IoU).

The algorithm output (see Figure 9a) resembles the general area and shape of the ground truth (see Figure 9b). However, as shown in Figure 9c, some false

positive and false negative predictions are present. In this sample, the algorithm obtained an IoU score of 85 % which reflects the good performance. Some noise is present in the image, and this could be removed using de-noising techniques. This result is significantly higher than the IoU of 64 % Çelik et al. obtained using the black-box EfficientNetB0 model.

Table 2 shows the surface area (in mm²) for the corrosion on the sample. The algorithm output produced a measurement of 5,081 mm², while the ground truth measurement was 5,467 mm². This indicates that the proposed method underestimated the area of corrosion staining with a relative error of -7 %. However, this metric includes false positives, which could lead to an overestimation of accuracy.

Table 2. Corrosion surface area. Algorithm output vs ground truth for sample 1.

	Pixel count	Surface area (mm ²)
Algorithm output	681,330	5,081
Ground truth	733,147	5,467

4.2.2 Dataset sample 2

Figure 10 displays the results of the proposed algorithm for the dataset sample 2. The algorithm output closely matches the ground truth, this is reflected by the high IoU score of 89 %. Table 3 shows the sample 2 surface area measurements. The total corrosion surface area for the algorithm was measured as 10,863 mm², this is close to the 11,798 mm² of the ground truth and results in a relative error of -8 %.

Table 3. Corrosion surface area. Algorithm output vs ground truth for sample 1.

	Pixel count	Surface area (mm ²)
Algorithm output	1,456,619	10,863
Ground truth	1,582,070	11,798

4.3 Discussion

While the algorithm's segmentation outputs generally align with the shape of the corrosion ground truth, they contain small holes and patches. Many of these patches correspond to areas with lighter staining than the surrounding corrosion. The human-defined ground truths classify these regions as corroded, but this involves a degree of subjective judgment. As a result, benchmarking becomes challenging, and the IoU score could improve if ground truths accounted for this variability.

Selective reflection enhances the contrast of corrosion in greyscale images, allowing for more information to be gathered. However, the RGB information is disregarded, and it may be beneficial to combine the proposed method with existing colour hue thresholding methods.

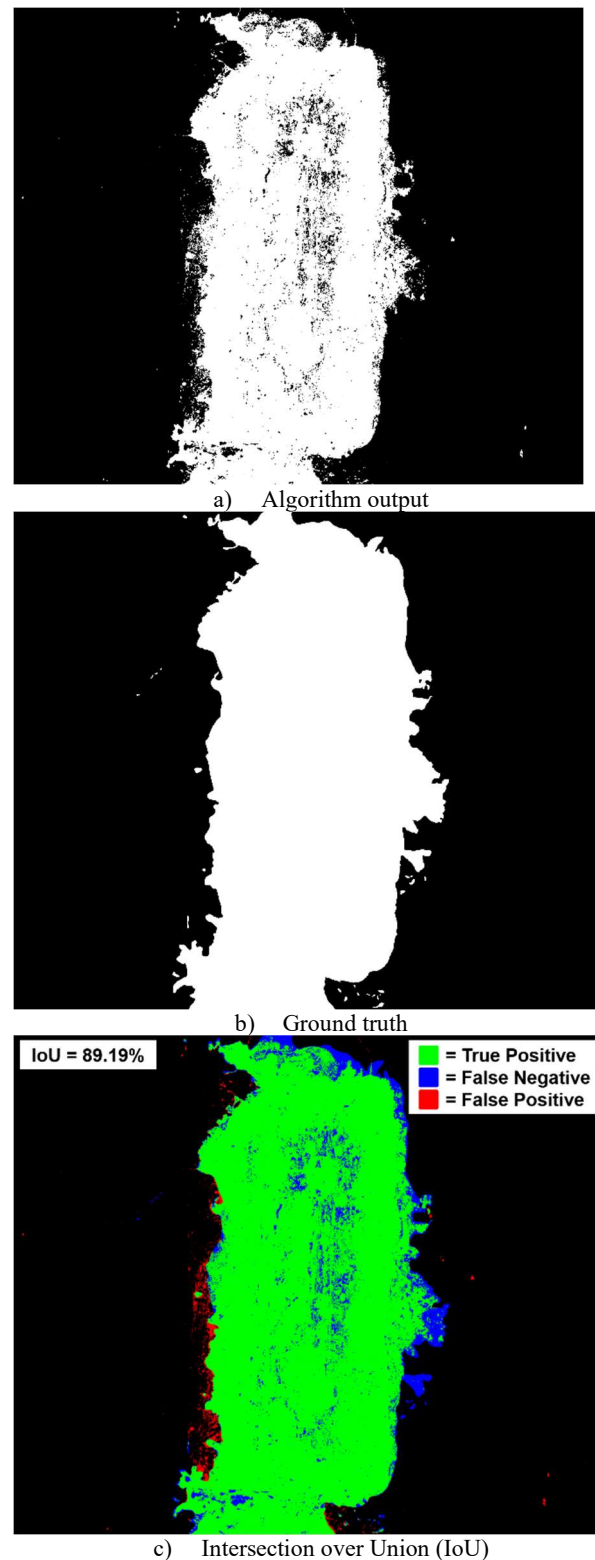


Figure 10. Results for dataset sample 2: a) Algorithm output; b) Ground truth; c) Intersection over Union (IoU).

5 Conclusion and future work

5.1 Conclusion

This paper demonstrated how selective reflection can be leveraged for concrete corrosion and exposed reinforcement detection and measurement. The results show that illuminating a concrete surface with blue light enhances the visibility of red corrosion, which absorbs the blue light, creating a stronger contrast in images for human review. Additionally, the paper introduces a corrosion pixel-level segmentation algorithm based on Otsu thresholding. As the algorithm takes greyscale images as an input, the improved corrosion-concrete contrast in the greyscale images from the blue lighting allows effective segmentation of corrosion and exposed reinforcement. Additionally, this provides use for greyscale cameras to interpret corrosion information in an image scene.

In testing, the algorithm obtained an IoU of at least 84 % compared to human-defined ground truths, across two laboratory dataset sample cases. While testing was conducted on only two dataset samples, the IoU results were significantly higher than other corrosion segmentation works in literature. The measured corrosion area closely matched ground truth values, with a maximum relative error of -8 %. The enhanced inspection images showcased in this work are human-interpretable and can provide more information for a human inspector. Additionally, the automated concrete inspection technique proposed in this research can provide human inspectors with a valuable new approach to improve inspection efficiency and ensure reinforced concrete asset longevity.

5.2 Future work

While the proposed method demonstrated strong performance, relying solely on greyscale images discards valuable colour information that could further enhance corrosion segmentation. Future research should explore corrosion segmentation techniques that incorporate RGB colour channel intensity variations under white illumination and blue illumination. Additionally, Lab (L: lightness; a: green-magenta; b: blue-yellow) colour space could be utilised.

The threshold value of 80 % of the Otsu thresholding value should be verified and optimised by conducting a full sensitivity analysis. Furthermore, the testing in this paper did not test for false positives when other red elements were present in the image scene, such as paint, aggregates, or steel components attached to the concrete. Additionally, the exposed reinforcement and corrosion are labelled under one segmentation class, meaning quantification of exposed reinforcement (length exposed, etc.) is not possible. To address these issues, future work should investigate the use of deep learning-based semantic segmentation networks.

Further validation is also needed. The proposed method should be quantitatively benchmarked against state-of-the-art corrosion segmentation techniques that utilise white lighting images. The corrosion surface area measurement should also be benchmarked against

human measurements. Finally, to assess real-world applicability, testing should be conducted on samples from real-world structures rather than solely on laboratory datasets.

6 References

- [1] F. Zhang, X. Xi, and S. Yang, "Research Progress in Corrosion Mechanism of Reinforced Alkali-Activated Concrete Structures," *Corros. Mater. Degrad.*, vol. 2, no. 4, Art. no. 4, Dec. 2021, doi: 10.3390/cmd2040034.
- [2] P. M. Calvi, E. Che, T. Sweet, L. N. Lowes, and J. W. Berman, "Data Collection Using Terrestrial Laser Scanners from the Shake-Table Test of a Full-Scale Reinforced Concrete Building," *J. Struct. Eng.*, vol. 150, no. 2, p. 04023219, Feb. 2024, doi: 10.1061/JSENDH.STENG-12627.
- [3] P. Stałowska, C. Suchocki, and M. Rutkowska, "Crack detection in building walls based on geometric and radiometric point cloud information," *Autom. Constr.*, vol. 134, p. 104065, Feb. 2022, doi: 10.1016/j.autcon.2021.104065.
- [4] S. Dorafshan and M. Maguire, "Bridge inspection: human performance, unmanned aerial systems and automation," *J. Civ. Struct. Health Monit.*, vol. 8, no. 3, pp. 443–476, Jul. 2018, doi: 10.1007/s13349-018-0285-4.
- [5] H. Dow, M. Perry, J. McAlorum, S. Pennada, and G. Dobic, "Skeleton-based noise removal algorithm for binary concrete crack image segmentation," *Autom. Constr.*, vol. 151, p. 104867, Jul. 2023, doi: 10.1016/j.autcon.2023.104867.
- [6] F. Çelik, P. Herbers, and M. König, "Image Segmentation on Concrete Damage for Augmented Reality Supported Inspection Tasks," in *Advances in Information Technology in Civil and Building Engineering*, S. Skatulla and H. Beushausen, Eds., Cham: Springer International Publishing, 2024, pp. 237–252. doi: 10.1007/978-3-031-35399-4_19.
- [7] Y. Xu, W. D. Qiao, Y. Q. Bao, H. Li, and Y. F. Zhang, "Pixel-level damage detection for concrete spalling and rebar corrosion based on U-net semantic segmentation," in *Bridge Maintenance, Safety, Management, Life-Cycle Sustainability and Innovations*, CRC Press, 2021.
- [8] V. Guru Prathap Reddy, T. Tadepalli, and R. Kumar Pancharathi, "Surface imaging based non-destructive assessment of concrete deterioration using hue-saturation-intensity colour space," *Measurement*, vol. 197, p. 111311, Jun. 2022, doi: 10.1016/j.measurement.2022.111311.
- [9] H.-W. Cho, H.-J. Yoon, and J.-C. Yoon, "Analysis of Crack Image Recognition

- Characteristics in Concrete Structures Depending on the Illumination and Image Acquisition Distance through Outdoor Experiments,” *Sensors*, vol. 16, no. 10, Art. no. 10, Oct. 2016, doi: 10.3390/s16101646.
- [10] J. McAlorum, H. Dow, S. Pennada, M. Perry, and G. Dobie, “Automated Concrete Crack Inspection With Directional Lighting Platform,” *IEEE Sens. Lett.*, vol. 7, no. 11, pp. 1–4, Nov. 2023, doi: 10.1109/LENS.2023.3327611.
- [11] H. Dow, M. Perry, S. Pennada, R. Lunn, and S. Pytharouli, “3D reconstruction and measurement of concrete spalling using near-field Photometric stereo and YOLOv8,” *Autom. Constr.*, vol. 166, p. 105633, Oct. 2024, doi: 10.1016/j.autcon.2024.105633.
- [12] Z. Ren, F. Fang, N. Yan, and Y. Wu, “State of the Art in Defect Detection Based on Machine Vision,” *Int. J. Precis. Eng. Manuf.-Green Technol.*, vol. 9, no. 2, pp. 661–691, Mar. 2022, doi: 10.1007/s40684-021-00343-6.
- [13] D. Chen, F. Kang, J. Chen, S. Zhu, and H. Li, “Effect of light source wavelength on surface defect imaging in deep-water concrete dams,” *NDT E Int.*, vol. 147, p. 103198, Oct. 2024, doi: 10.1016/j.ndteint.2024.103198.
- [14] B. Özcan, R. Schwermann, and J. Blankenbach, “A Novel Camera-Based Measurement System for Roughness Determination of Concrete Surfaces,” *Materials*, vol. 14, no. 1, Art. no. 1, Jan. 2021, doi: 10.3390/ma14010158.
- [15] Y. Blikharskyy and A. Pavliv, “Formation of a Complete Stress-Strain Curve of Concrete Using Digital Image Corellation,” Jun. 30, 2021, *Social Science Research Network, Rochester, NY*: 3887772. Accessed: Feb. 12, 2025. [Online]. Available: <https://papers.ssrn.com/abstract=3887772>
- [16] N. Otsu, “A Threshold Selection Method from Gray-Level Histograms,” *IEEE Trans. Syst. Man Cybern.*, vol. 9, no. 1, pp. 62–66, Jan. 1979, doi: 10.1109/TSMC.1979.4310076.